The cosmic ray energy spectrum around the knee measured with the GAMMA array at Mt. Aragats

A P Garyaka[1], **R M Martirosov**[1], **J Procureur**[2], **E A Mamidjanian**[3] **and V S Eganov**[1]

[1] Yerevan Physics Institute, Br. Alikanian St 2, 375036 Yerevan, Republic of Armenia
[2] Centre d' Etudes Nucléaires de Bordeaux-Gradignan, Université de Bordeaux, 1 rue du Solarium, 33175 Gradignan-Cedex, France
[3] P.N. Lebedev Institute, Leninsky pr. 56, Moscow 117924, Russia

Abstract
Experimental data on EAS characteristics with $N_e > 10^5$ are used to calculate the so-called α_e-parameter which is directly connected with the energy of the primary cosmic ray radiation. It is shown that the distribution of showers selected by a constant value of this parameter is isotropic, and the measurement of the α_e-spectrum is a direct way to obtain the primary energy spectrum. Using the α_e-parameter, the primary all-particle energy spectrum of the cosmic radiation in the knee region is obtained. The energy spectrum is compared with the corresponding data of other experiments.

1. Introduction

The energy spectrum of the primary cosmic radiation comprises more than 12 orders of magnitude in energy scale and extends to enormous energies up to 10^{20} eV, the highest energies of individual particles in the universe. The most conspicuous feature of the energy spectrum is a distinct change of the spectral index of the power-law fall-off around 10^{15} eV, called the *knee*. Discussions about the origin of the *knee* in this region began at once after the discovery of this phenomenon more than 40 years ago [1] and continued until the present time. Up until now it has not been clear whether the *knee* is due to magnetic confinement of the cosmic rays in our galaxy or is the consequence of some characteristics of the cosmic ray sources. There is also the hypothesis of the change of ultra-high energy hadron interactions in the Earth's atmosphere [2]. At present, any of the hypotheses are feasible, because there is no unequivocal explanation of such a change in the shape of the primary spectrum. Furthermore, it is important to underline that the uncertainty of the experimental data about the primary mass composition begins precisely in the *knee* region of the primary energy or EAS size spectra.

For all these reasons, one of the basic tasks of practically all ground experiments working in this energy region, $(10^{15}–10^{17})$ eV, is to obtain reliable data about the energy spectrum and mass composition of the primary cosmic rays. In fact, most of the experiments, registering simultaneously all components of EAS generated in the Earth's atmosphere by the primary

cosmic rays are involved in solving these problems [3–5]. But despite plentiful experimental data obtained over many years, there are significant divergences in the results obtained by the different experiments. The reason for these discrepancies can be the various depths of the atmosphere on which the installations are placed (from sea level up to 5000 m above sea level (a.s.l.)), and essential differences in techniques used for the analysis of the experimental data.

At present there are a few methods to determine the primary particle energy and, in particular, for experiments using indirect methods for detection of the extensive air showers at ground level. Some of them were discussed in [6], which is particularly devoted to this question. These methods are based, essentially, on the EAS electron number N_e. Unfortunately, N_e is strongly sensitive to fluctuations in the EAS longitudinal development (especially for installations located at sea level) and the connection $N_e - E_0$ strongly depends on the type of the primary particle. In the well-known formula [7] of the connection between E_0 and N_e, $E_0 = a N_e^b$, both parameters a and b depend on the type of the primary particles generating the EAS.

Moreover, according to [7], parameter b also depends on the arrival direction of the incoming primary particle. This situation certainly complicates the estimation of the primary particle energy using N_e only. This problem has recently been discussed extensively in many papers, and some other methods to evaluate the primary energy were proposed. But it is obvious that any new method must not be sensitive to the model of hadronic interaction for analysis and interpretation of the experimental data.

Along these lines, in [8] a new method was proposed to determine the primary energy by measuring N_e for each shower at detection level and after an additional absorber 100 g cm^{-2}. Reference [9] discusses the possibilities of an estimation of the primary energy using the ratio N_μ/N_e for each event. In the KASCADE experiment [10], the muon density spectrum of the EAS is used to obtain the primary spectrum. A non-parametric regression method for evaluation of the primary particle energy is used in [11].

The idea to use for the primary energy estimation not only the electron number N_e, but also the EAS electron lateral distribution function, has been discussed. In this context, a new method was proposed some years ago specifically for experiments at mountain altitudes [12, 13]. In this way, it is possible to select showers generated by primaries with different masses but with the same primary energy. The main interest of this method is that the energy determination is performed using only the lateral densities of electromagnetic particles. It is well known that these particles on the ground are much more easily registered than hadrons or underground muons, so that the experimental data obtained have a better accuracy. It is important to note that this new method is not dependent on the hadronic model chosen in simulation for the high energy nuclei–nuclei interaction [14]. During recent years this method was specifically adapted for the GAMMA array.

In this paper we present the all-particle energy spectrum of the primary cosmic radiation in the energy region (10^{14}–10^{16}) eV, including the *knee*, obtained with the GAMMA array data at Mt. Aragats [15, 16]. We used this new method, which means that EAS are grouped together by constant energy of primaries and not by constant sizes, N_e.

2. Experiment

2.1. The GAMMA array

Located on the hillsides of Mt. Aragats in Armenia (3200 m a.s.l.), the GAMMA array is a part of the ANI project. A schematic view of the array is shown in figure 1.
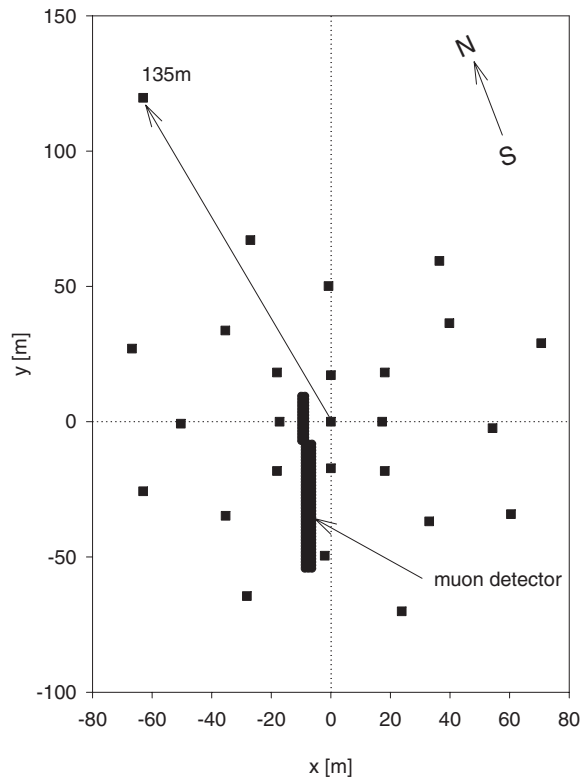
Figure 1. The layout of the GAMMA installation.

The GAMMA array consists of a surface part to register the EAS electromagnetic component and of underground detectors for detection of the EAS muons.

On the surface, 75 plastic scintillation detectors are placed at 25 surface points (three detectors at each point). The effective surface of each detector is 1 m². These points are distributed over the full area of $\approx 1.5 \times 10^4$ m². The presence of the three detectors at each point allowing us to obtain an average density for each point, considerably improves the accuracy of determination of the electron lateral distribution function. The maximal distance of detectors from the array centre is 135 m, where 20 identical detectors are placed.

The underground muon scintillation hodoscope consists of 150 similar detectors for the registration of the EAS muon component. The muon energy thresholds are 2.5 GeV and 5.0 GeV.

Moreover, the surface scintillation hodoscope of the GAMMA array is equipped with a 25-channel chronotron system [16] (one channel for each surface point).

The accuracy of the EAS parameter estimations is as follows:

- coordinates of EAS axes: ΔX, $\Delta Y < 3$ m (for $R < 40$ m),
- zenith and azimuth angles: $\sigma_\theta \simeq 1.5°$, $\sigma_\varphi \simeq 8°$,
- shower size: $\sigma(N_e)/\langle N_e \rangle \leqslant 20\%$.

A more detailed description of the GAMMA array is presented in [17].

In this paper, the GAMMA experimental data obtained from August 1998 to June 2001 are analysed. The effective running time used for this analysis is $\sim$350 days. The total number of EAS with $N_e > 10^5$ and with zenith angle $\theta < 30°$ is $\sim$800 000.
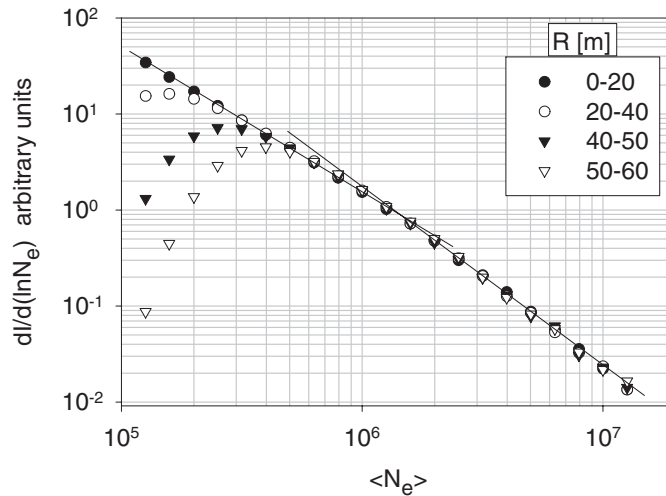
Figure 2. The differential spectra versus number of electrons N_e at zenith angles $\theta < 30°$. The lines are the fits of experimental points before and after the knee.

2.2. Efficiency of the shower selection

It must be noted that the efficiency of shower registration is not uniform on the GAMMA array surface part and depends on the shower size, because of the irregular distribution of the scintillation detectors. Detectors are more rarefied on the periphery than in the centre. Consequently, the central part registers small size showers with better efficiency than on the periphery. Moreover, there are some significant differences between the Z coordinates of individual detectors, reaching in some places 18 m, because of the GAMMA array disposition. This peculiarity of the array also influences the efficiency of the shower selection, especially for the estimation of the shower angular characteristics.

In order to check the efficiency of the EAS registration on the entire GAMMA array area, we obtained differential size spectra normalized per square metre for showers with axes located between different circles. Figure 2 shows the differential size spectra for circles with radii $R = 0$–20 m, 20–40 m, 40–50 m and 50–60 m at zenith angles $\theta < 30°$.

It can be seen in this figure that the installation selects showers inside of these radii with different efficiencies. At $N_e > 10^6$ the showers are registered with equal 100% efficiency over the full range of $R = (0$–60) m. The smaller size showers ($N_e < 6 \times 10^5$) are registered effectively inside the radius of 20 m. We would like to underline that in comparison with experimental data represented in [17], the statistics have been considerably improved. This allows us to use the differential approach to analyse the experimental data depending on the location of the EAS axis and shower size.

3. The parameter $\alpha_e(70)$ as the primary energy estimator

3.1. Definition of the $\alpha_e(70)$ parameter and comments

As was specified in the introduction, it is fundamental to select showers generated by primaries with different masses but with the same primary energy, and not with the same size, as is

usually done. For this purpose we proposed some years ago [12] for mountain altitude, $(t_0 = 700 \text{ g cm}^{-2})$, to select showers according to a fixed value of the α_e-parameter:

$$\alpha_e(70) = 70^2 \rho_e(70)/f_{\text{NKG}}(10, S_{5-70}),$$

where:

- $\rho_e(70)$ is the density of charged particles at 70 m from the shower axis,
- f_{NKG} is the well-known Nishimura–Kamata–Greisen function [18],
- S_{5-70} is the local age[4] estimated from densities at 5 and 70 m from the shower axis.

Let us recall that this parameter is 'ad hoc' and defined in such a way that its energy dependence is the same for all primary masses. For example, the value of the parameter 10 in the NKG formula $f_{\text{NKG}}(10, S_{5-70})$ has no physical meaning but was chosen to optimize this primary mass independence only. In fact, to improve its efficiency we have been obliged to slightly modify the values of parameters in the α_e definition. For example, in a recent work [19], we showed that this parameter α_e is very weakly dependent on the model of hadronic interaction at very high energies. However, we slightly modified the definition of α_e to optimize its independence from the model of nuclear interactions as follows:

$$\alpha_e(135) = 135^2 \rho_e(135)/f_{\text{NKG}}(3, S_{25-135}).$$

The experiment GAMMA gives us the possibility of applying our method of selection of the showers with constant energy to a real experiment. However, the analysis of experimental results highlighted two difficulties:

- in spite of the existence of a density detector with a large effective area (20 m^2) located at 135 m from the centre of the installation, the experimental fluctuations of the charged particle density at this distance are more significant than those provided by the simulation code (CORSIKA version 5.20) with the QGSjet model of hadronic interactions [20];
- the lack of precision of $\rho_e(135)$ implies an inaccurate estimation of the local age parameter S_{25-135}, obtained using densities at 25 and 135 m from the shower axis.

Moreover, any error in the estimation of the shower axis location generates an uncertainty in S_{25-135} and, consequently, in the evaluation of α_e. This is why, in the definition of α_e we replaced the local age S_{25-135} by the Nishimura–Kamata–Greisen age parameter, S_{NKG}, [19]. We made sure that the experimental electron lateral distributions as well as the simulated ones are described by the NKG function with high accuracy for distances up to 120 m. Let us recall that this parameter is obtained by fitting the lateral density of the charged particles with the help of the Nishimura–Kamata–Greisen function using measured densities at many distances from the shower axes. Naturally the parameter S_{NKG} is much less sensitive to the EAS fluctuation than the local age parameter. After this change the parameter α_e was defined as

$$\alpha_e(70) = 70^2 \rho_e(70)/f_{\text{NKG}}(1, S_{\text{NKG}}).$$

The dependence of the primary particle energy on the parameter $\alpha_e(70)$ is presented in figure 3 for showers generated by proton and iron nuclei.

This figure shows that the existing proportionality between the parameter $\alpha_e(70)$ and primary energy is independent of the mass of the primary projectiles. It must be noted that the showers were simulated with random zenith angles within the interval $\theta \in [0, 30]^\circ$. The following expression was obtained for this dependence:

$$\langle E_0 \rangle = 5.18 \times 10^3 \alpha_e(70) \text{ [GeV]}.$$

---

[4] If $\rho_e(r_1)$ and $\rho_e(r_2)$ are the densities of charged particles at distances r_1 and r_2 from the shower axes, then: $S_{r_1-r_2} = \ln\left[\frac{\rho_e(r_1)}{\rho_e(r_2)}\left(\frac{r_1}{r_2}\right)^2\left(\frac{r_1+r_0}{r_2+r_0}\right)^{4.5}\right] \Big/ \left[\frac{r_1(r_1+r_0)}{r_2(r_2+r_0)}\right]$, where r_0 is the Moliere radius.
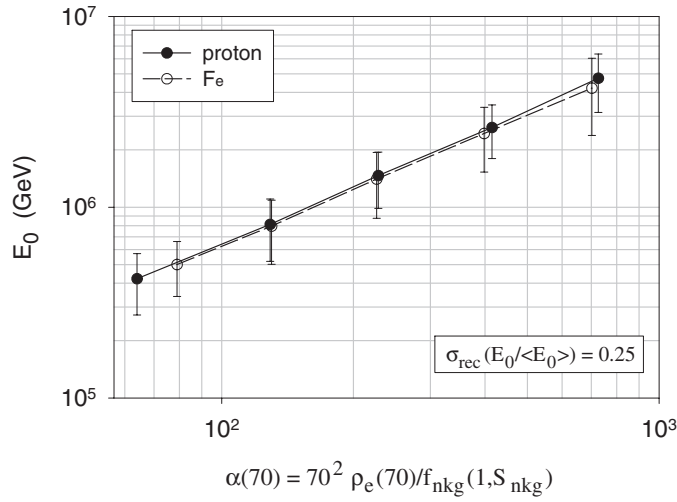
Figure 3. The primary particle energy versus the parameter $\alpha_e(70)$ for proton and iron showers (simulation). The error bars are the standard deviations.

It is also important to emphasize that for this figure and for the next we included in the simulation model the uncertainties due to the experimental acceptance requirements. Indeed, because of the experimental conditions of detection, the error in the experimental determination of $\alpha_e(70)$ implies that $\sigma_{rec}(K_{\alpha_e}) = 0.25$, where $K_{\alpha_e} = \alpha_e(70)/\langle\alpha_e(70)\rangle$. Thus, the total uncertainty in $\alpha_e(70)$ becomes $\sigma_{total}(K_{\alpha_e}) = \sqrt{\sigma_{dev}^2(K_{\alpha_e}) + \sigma_{rec}^2(K_{\alpha_e})}$, where σ_{dev} is the standard deviation due to fluctuations in the shower development.

In order to check the consistency of our method of shower selection, we show in figure 4 the dependence of the shower size versus the primary particle energy, on one hand, and of the $\alpha_e(70)$ parameter, on the other. This comparison has been made for the normal composition of the primary cosmic radiation, namely,

proton: 40%, α: 21%, light-nuclei ($\langle A \rangle = 14$): 14%, medium-nuclei ($\langle A \rangle = 26$): 13%

and heavy-nuclei ($\langle A \rangle = 56$): 12%.

Figure 4 confirms that selecting showers with $\alpha_e(70)$ constant is equivalent to selecting them with the primary energy constant in the energy range $[5 \times 10^5 – 10^7]$ GeV.

3.2. Comparison between experimental and simulated data

All simulated data discussed in this paragraph are obtained for the normal primary mass composition presented above.

The parameter $\alpha_e(70)$ is defined using measurements of the charged particle densities. Therefore, it is important to have a good agreement between simulated and experimental densities for the whole range of r. Figure 5 presents the lateral distributions of charged particles for showers selected with constant size in the following intervals: $[1.78, 3.16] \times 10^5$, $[5.63, 10.00] \times 10^5$ and $[17.78, 31.62] \times 10^5$ up to $r = 120$ m.

One can see in this figure the good agreement between measurements and simulation data, in particular, at a distance of 70 m from the shower axis.

As noted above, the definition of $\alpha_e(70)$ takes into account the age parameter S_{NKG}. It is one of the main characteristics of the EAS electromagnetic component, because this parameter
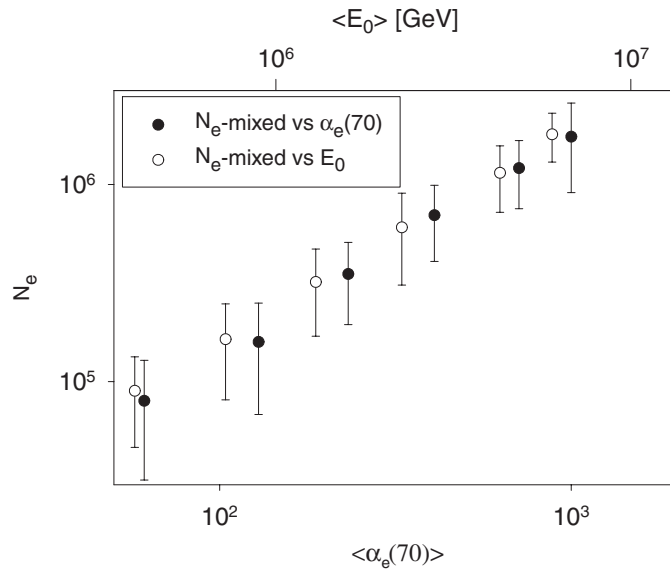
Figure 4. The dependence of the shower size N_e on one hand versus the primary energy E_0 and, on the other, versus the parameter $\alpha_e(70)$. These results are from simulation and for the standard mixed primary composition. The error bars are the standard deviations.
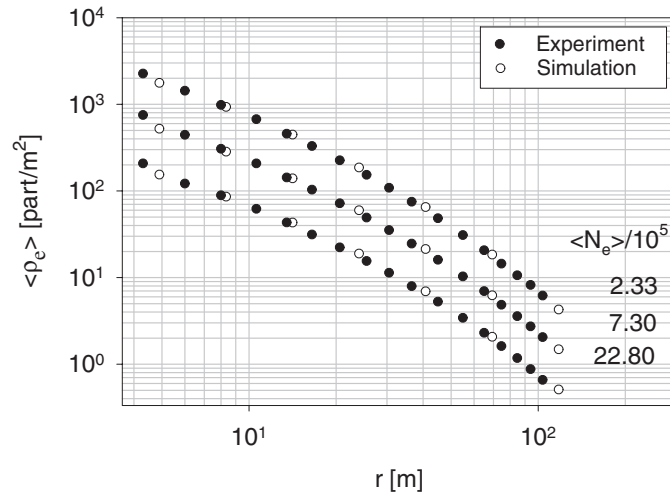
Figure 5. Experimental and simulated lateral distributions of electromagnetic particles for the showers selected with constant size N_e. The statistical errors are smaller than the symbols used and cannot be seen.

represents the shape of the lateral distribution of the electron density. According to the $\alpha_e(70)$ definition, this parameter is of special importance for the determination of the primary particle energy using the method presented in this paper. Taking into account some peculiarities of the GAMMA array (for example, non-uniformity of the whole surface area) the shower discrimination using S_{NKG} is quite possible. In order to check this effect we obtained the experimental S_{NKG} for different bins in N_e and belts of the shower axis selection (see table 1).
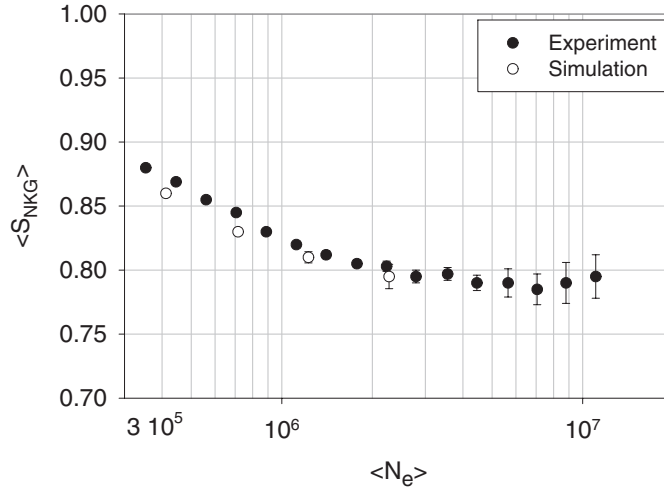
Figure 6. The experimental and simulated average age parameter $\langle S_{NKG} \rangle$ versus the shower size $\langle N_e \rangle$. The bars are the statistical errors.

Table 1. Average values of the experimental S_{NKG} and standard deviation for different $\langle N_e \rangle$ and belts.

|	$\langle N_e \rangle$				
$R(m)$	1.76×10^5	3.16×10^5	15.4×10^5	47.5×10^5	173.1×10^5
0–20	0.93 ± 0.14	0.89 ± 0.13	0.82 ± 0.09	0.81 ± 0.09	0.81 ± 0.10
20–40	0.93 ± 0.15	0.89 ± 0.12	0.82 ± 0.10	0.80 ± 0.10	0.81 ± 0.10
40–50	0.95 ± 0.14	0.90 ± 0.13	0.82 ± 0.12	0.80 ± 0.11	0.82 ± 0.09
50–60	0.99 ± 0.14	0.90 ± 0.13	0.82 ± 0.12	0.80 ± 0.11	0.82 ± 0.11

It can be seen in this table that $\langle S_{NKG} \rangle$ remains constant for sizes larger than 3.16×10^5 in any radius of shower selection up to $R = 60$ m.

In figure 6 the dependence of S_{NKG} on the shower sizes is shown with statistical errors. Again the agreement between experimental measurements and the values obtained by simulation is very good.

In figure 7 the values of $\alpha_e(70)$ for EAS selected with fixed size are presented. Once more the agreement between experimental and simulated data is excellent.

As shown previously [17, 19, 21] and confirmed in this work, there is good agreement between the average values of the simulated and experimental data. However, in order to obtain an undistorted primary particle energy spectrum it is insufficient to have agreement of the EAS average characteristics and, in particular, the S_{NKG} versus $\langle N_e \rangle$ dependence. It is also necessary to have agreement of the age parameter distributions for different bins in N_e.

Figure 8 shows the experimental and simulated distributions of the age parameter for two given shower sizes. In the simulated results, the total standard deviation is obtained by superposition of the relative uncertainties of the fluctuations in the shower development and of the experimental conditions of detection. The shape is Gaussian with a quite reasonable relative standard deviation ($\sim$11%).
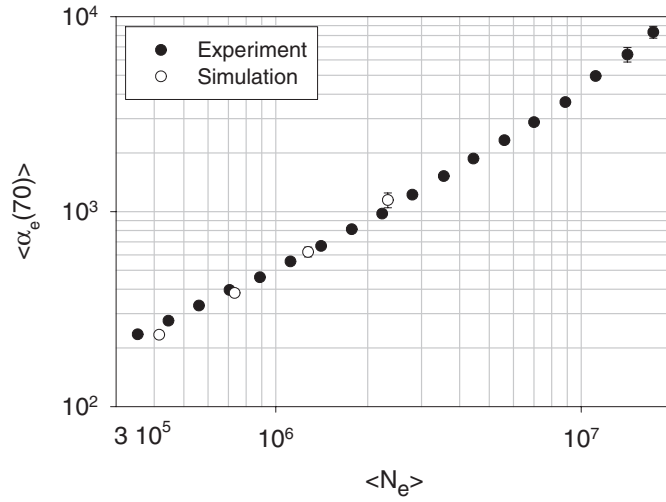
Figure 7. The dependence of the parameter $\alpha_e(70)$ versus the shower size (experiment and simulation). The bars are the statistical errors.

3.3. Properties of EAS selected at given parameter $\alpha_e(70)$

The $\alpha_e(70)$ parameter allows us to select EAS generated by primaries with the same energy E_0. These selected showers must be uniformly distributed within the angular interval used. This is a necessary requirement for any primary energy estimator, and it would be interesting to test various energy estimators in this way. On this point, we would like to underline that showers selected by constant size N_e do not have a uniform angular distribution and have steep angular dependence. Showers with number of electrons $N_e > 10^5$, number of muons $N_\mu > 5 \times 10^3$ and zenith angles $\theta < 45°$ are included in our analysis.

Figure 9 presents the experimental angular distributions of the showers selected at given values of the shower size N_e, the number of muons N_μ and two given values of the parameter $\alpha_e(70)$.

It can be seen that up to a zenith angle value $\theta = 30°$ the distribution of showers selected by $\alpha_e(70) \geqslant 700$ and $\alpha_e(70) \geqslant 1000$ is close to isotropic, in contrast to distributions of the showers selected at given values of the shower size N_e or the number of muons N_μ. This is the proof that the showers selected by fixed parameter $\alpha_e(70)$ have the same energy independent of the mass of the primary particles.

4. The primary energy spectrum

The energy spectrum for all primary particles is obtained by using the values of the experimental $\alpha_e(70)$ spectrum and the coefficient $K = 5.18 \times 10^3$ GeV derived from the data of figure 3. Errors in the determination of E_0 are the sum of the errors of the method itself and the experimental errors in the measurement of $\rho_e(70)$ and the determination of S_{NKG}. The error of E_0 strongly depends on the accuracy of S_{NKG}:

$$\Delta E_0 / E_0 = 4.72 \Delta S_{\text{NKG}}$$

and increases with N_e. This relation is easy to obtain by substituting in the $\alpha_e(70)$ definition the expressions for $\rho_e(70)$ and $f_{\text{NKG}}(1, S_{\text{NKG}})$. The lower bound of the all-particle energy
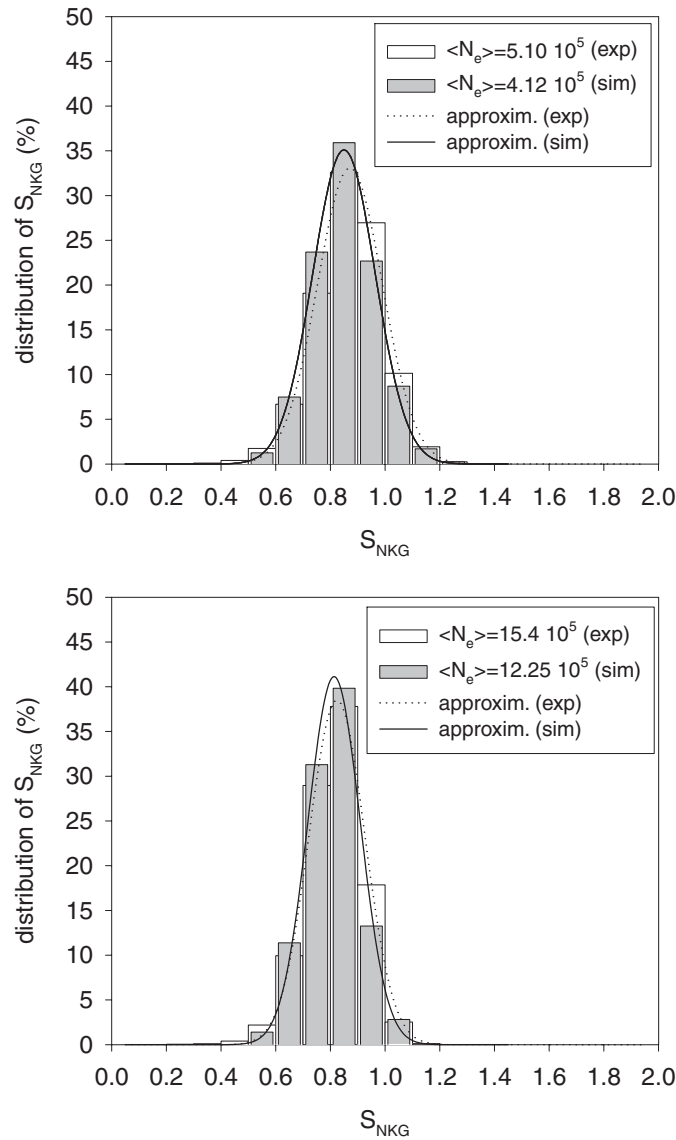
Figure 8. Experimental and simulated distributions of the age parameter S_{NKG} for different shower sizes $\langle N_e \rangle$.

spectrum derived by the presented method is $E_0 \sim 1.5 \times 10^{15}$ eV, which is very close to the knee energy region.

The accuracy of E_0 is $\sim 25\%$ around the knee. Figure 10 presents the primary energy spectrum obtained with the GAMMA array in comparison with schematic approximations of results from some other experiments. We would like to underline that the bumps observed at $E_0 \sim 3 \times 10^7$ GeV are not connected to any methodical effects. Before the knee our spectrum is steeper than others. However, because the number of points are few, any definitive conclusion would be meaningless. After the knee its slope is in agreement with most of them
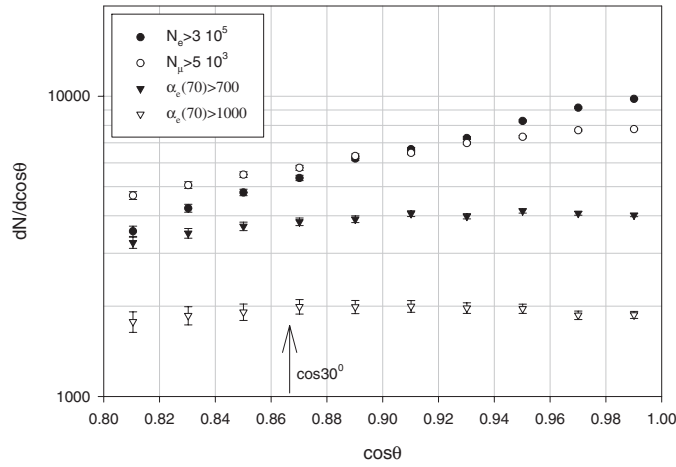
Figure 9. Experimental angular distributions of N_e and N_μ for showers selected at given values of $\alpha_e(70)$. The bars are the statistical errors.
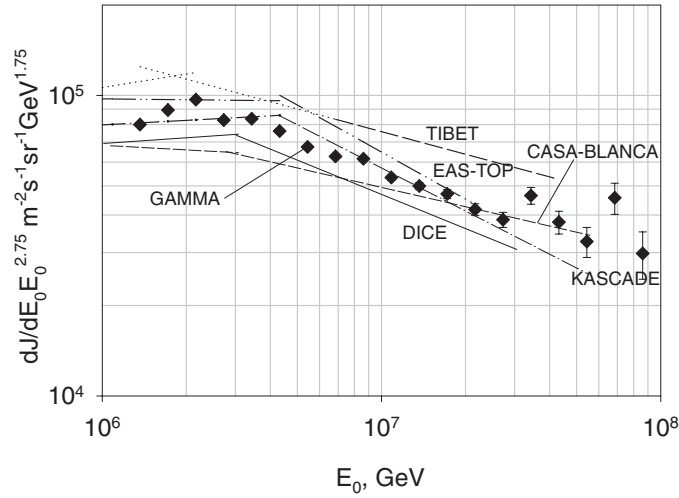
Figure 10. The primary energy spectrum in comparison with results from other experiments. The lines are fitting data of different experiments (see compilation in [22]). The bars are the statistical errors.

with $\gamma = 3.10 \pm 0.1$. It can be seen that our spectrum after the knee is very close to the data of the KASCADE experiment.

5. Conclusions

Using the GAMMA array experimental data, we show the applicability of the new primary energy estimator $\alpha_e(70)$ for the determination of the primary energy spectrum in the range 10^{15}–3×10^{16} eV. Obtained in this manner, the primary energy spectrum does not contradict the results from other experiments.

It is important to note that the showers selected by the $\alpha_e(70)$ criterion have an isotropic angular distribution at zenith angle values $\theta < 30°$ in contrast to N_e and N_μ distributions.

The presented energy spectrum is a spectrum of all kinds of primary particles (nuclei), obtained without any hypothesis about the primary mass composition, but on the assumption of the lack of the sharp changes in the hadron–nuclei interaction. We would like to underline that the bump observed at $E_0 \sim 3 \times 10^7$ GeV is not connected to any methodical effects.

As a next step, we plan to estimate the mass composition of the primary cosmic radiation in this energy region using a multi-parameter analysis of the EAS components.

Acknowledgments

References

[1] Kulikov G V and Khristiansen G B 1958 *JETP* **35** 635
[2] Nikolsky S I and Romakhin V A 2000 *Phys. At. Nuclei* **63** 10, 1799
[3] Glasmacher M A K *et al* 1999 *Proc. 26th Int. Cosmic Rays Conf. (Durban)* vol 3 p 129
[4] Kampert K-H *et al* 1998 *Proc. 16th European Cosmic Ray Symp. (Alcala)* p 547
[5] Navarra G *et al* 1999 *Nucl. Phys.* B **60** 105
[6] Cortina J *et al* 1997 *J. Phys. G: Nucl. Part. Phys.* **23** 1733
[7] Martinez S *et al* 1995 *Nucl. Instrum. Methods* A **357** 579
[8] Boss E G *et al* 2001 *Proc. 27th Int. Cosmic Rays Conf. (Hamburg)* p 269
[9] Capdevielle J-N *et al* 1991 *Proc. 22nd Int. Cosmic Rays Conf. (Dublin)* vol 4 p 409
[10] Haungs A *et al* 2001 *Proc. 27th Int. Cosmic Rays Conf. (Hamburg)* p 63
[11] Chilingaryan A A *et al* 2001 *Proc. 27th Int. Cosmic Rays Conf. (Hamburg)* p 93
       Roth M *et al* 2001 *Proc. 27th Int. Cosmic Rays Conf. (Hamburg)* p 88
[12] Procureur J and Stamenov J N 1995 *Nucl. Phys.* B **39** A 242
[13] Martirosov R *et al* 1995 *Nuovo Cimento* A **108** 3 299
[14] Brankova M *et al* 1997 *Proc. 25th Int. Cosmic Rays Conf. (Durban)* vol 4 p 81
[15] Arzumanyan S A *et al* 1995 *Proc. 24th Int. Cosmic Rays Conf. (Rome)* vol 1 p 482
[16] Volkov A E *et al* 1997 *Izv. Akad. Nauk SSSR Ser. Fiz.* **3** 529
[17] Eganov V S *et al* 2000 *J. Phys. G: Nucl. Part. Phys.* **26** 1355
[18] Cocconi G 1961 *Handbuch der Physik* XLVI/1 ed S Flügge (Berlin: Springer) p 215
[19] Brankova M *et al* 1998 *Proc. 16th European Cosmic Rays Symp. (Alcala de Henares)* p 493
[20] Heck D *et al* 1998 *Kernforschungszentrum, Karlsruhe* FZKA 6019
[21] Garyaka A P, Martirosov R M, Procureur J and Zazyan M Z 2001 *Nucl. Phys.* B **97** 263
[22] Castellina A 2001 *Nucl. Phys.* B **97** (Proc. Suppl.) 35